

An Active Control Method for Chatter Suppression in Thin Plate Turning

Haifeng Ma[®], Jiajie Guo[®], *Member, IEEE*, Jianhua Wu, *Member, IEEE*, Zhenhua Xiong[®], *Member, IEEE*, and Kok-Meng Lee[®], *Fellow, IEEE*

Abstract—This paper presents an active control method, consisting of an adaptive sliding-mode controller (ASMC) and a displacement field reconstruction (DFR) method, for chatter suppression in turning of thin-walled workpieces (such as compressor disks and casings in aircraft engines) where low workpiece stiffness renders machining with potential regenerative chatter. Due to the presence of multimodal dynamics, variant modal parameters, and measurement difficulties, active chatter control of thin plate turning has been challenging. Unlike existing controls based on a lumped-parameter single degree-of-freedom cutting model, a distributed-parameter dynamic model of a rotating thin plate with multiple vibration modes is used to analyze the machining stability with the designed controller. Moreover, model parameters of the plate are not needed to construct the controller. The DFR is employed to capture the plate dynamic behavior for feedback to the ASMC during turning, overcoming the long existing difficulties to measure plate vibration at the cutting point. A fast tool servo is utilized in the control implementation. Theoretical analyses, numerical simulations, and experimental evaluation on a lathe demonstrate that chatter in thin plate turning can be effectively attenuated with the proposed active control method.

Index Terms—Active control, displacement field reconstruction (DFR), distributed-parameter system, regenerative chatter, thin plate turning.

Manuscript received April 21, 2019; revised June 16, 2019 and June 19, 2019; accepted June 20, 2019. Date of publication June 26, 2019; date of current version January 16, 2020. This research was supported in part by the National Basic Research Program of China under Grant 2013CB035800, in part by the Program of Shanghai Subject Chief Scientist under Grant 18XD1401700, in part by the National Science Foundation of China under Grant 51805327, and in part by U.S. National Science Foundation under Grant CMMI-1662700. Paper no. TII-19-1485. (Corresponding author: Zhenhua Xiong; and Kok-Meng Lee.)

H. Ma is with the Key Laboratory of High Efficiency and Clean Mechanical Manufacture of MOE, School of Mechanical Engineering, Shandong University, Jinan 250061, China, and also with the State Key Laboratory of Mechanical System and Vibration, School of Mechanical Engineering, Shanghai Jiao Tong University, Shanghai 200240, China (e-mail: MaHaifeg@sjtu.edu.cn).

J. Guo is with the State Key Laboratory of Digital Manufacturing Equipment and Technology, School of Mechanical Science and Engineering, Huazhong University of Science and Technology, Wuhan 430074, China (e-mail: jiajie.guo@hust.edu.cn).

J. Wu and Z. Xiong are with the State Key Laboratory of Mechanical System and Vibration, School of Mechanical Engineering, Shanghai Jiao Tong University, Shanghai 200240, China (e-mail: wujh@sjtu.edu.cn; mexiong@sjtu.edu.cn).

K.-M. Lee is with the George W. Woodruff School of Mechanical Engineering, Georgia Institute of Technology, Atlanta, GA 30332-0405 USA (e-mail: kok-meng.lee@me.gatech.edu).

Color versions of one or more of the figures in this paper are available online at http://ieeexplore.ieee.org.

Digital Object Identifier 10.1109/TII.2019.2924829

I. INTRODUCTION

REGENERATIVE chatter is one of the most detrimental phenomena in machining processes characterized by large vibration and high-level noise [1]. The occurrence of regenerative chatter induces loss of dimensional accuracy, reduces material removal rate (MRR), causes poor surface finish, and increases tool wear. With the ever-growing demand for good-quality products and high-efficient manufacturing, the need to develop chatter suppression techniques becomes critical and pressing for modern manufacturing industry [2]–[5].

Most existing chatter suppression methods are classified as passive techniques. One typical way is to constrain/optimize process parameters (spindle speed, feed rate, or width of cut) to achieve a stable working point [6]. Although chatter can be avoided by parameter regulation, the domain of stable operation is not enlarged by this methodology; hence, the manufacturing productivity is still limited. Passive chatter suppression techniques that adopt tuned mass dampers (TMDs) [7] or vibration absorbers [8] have also been used to dissipate the energy of chatter vibrations. However, absorbers require special procedures in industry [1] to ensure accurate tuning of their natural frequencies for acceptable performance. Dampers also suffer some drawbacks: large space is required at critical locations; and the damping effect is limited with variable properties of system dynamics. Hence, passive dampers and absorbers lack robustness to changing machining conditions.

On the contrary, active chatter suppression schemes (with suitable sensors/actuators installed on the spindle or tool holder) have demonstrated potentials to improve machine tool performances. Closed-loop control systems can be established to properly regulate the self-excitation dynamics, and hence to enlarge the domain of stable operation region in the stability lobe diagram [1]. Ganguli et al. [9] and Munoa et al. [10] demonstrated the effectiveness of active damping methods with direct velocity feedback for turning and milling processes. These methods can mitigate chatter with low computational requirements, and guarantee the machining stability with collocated actuators/sensors. In order to stabilize the spindle of a milling machine, Dohner et al. [11] developed an active control system employing a linear quadratic Gaussian controller with piezoelectric actuators. Mei [12] analytically investigated active chatter suppression (designed from a wave standpoint to absorb chatter vibration energy) for boring processes with a nonrotating tool. Chen et al. [4] designed chatter control approaches employing μ -synthesis for speed-independent,

1551-3203 © 2019 IEEE. Personal use is permitted, but republication/redistribution requires IEEE permission. See http://www.ieee.org/publications_standards/publications/rights/index.html for more information.

speed-specified, and speed-interval situations, respectively. The speed-interval chatter controller proposed in [4] was adopted by van Dijk et al. [5] for a high-speed milling spindle fully supported by active magnetic bearings. Monnin et al. [13] proposed two optimal control strategies to minimize the influence of cutting forces on tooltip vibrations, which were embedded in active magnetic bearings integrated into a spindle unit. Chen et al. [14] designed an adaptive control strategy to compensate the regenerative effect, especially for high-speed milling cases. Wu et al. [3] developed active controllers for chatter mitigation in milling processes by considering input constraints. Ma et al. [15] presented a dynamic output feedback controller for chatter suppression in turning processes, where only displacement measurement was required by the controller. A different perspective assuming that chatter is originated from flexible workpieces (WPs) was presented in [16] and [17], where piezoelectric actuators and sensors for implementing active damping to suppress chatter in milling were attached on the stationary WPs. However, this methodology is not suitable for machining of rotating WPs.

Although a lot of researches have been done on active chatter suppression, it remains a challenging task in turning of thin plates due to the following difficulties: 1) Thin or flexible component (plate) is a spatially distributed system and contains infinite number of vibration modes, so its cutting process is featured with multimodal machining dynamics. However, current active controller designs are generally based upon a simplified lumped-parameter single degree-of-freedom (DOF) cutting model. Consequently, only a single mode is suppressed and the remaining modes may be excited, resulting in a spill-over problem [17]. Although Mei [12] presented an active controller in view of a distributed boring bar model, it was proposed for one-dimensional structures and not suitable for the scenario involving thin or flexible WPs (plates). Moreover, only one dominating mode was considered in [12] to analyze and test the stability of the controller. 2) Workpiece parameters (i.e., mass, stiffness, and damping) vary greatly with the changing of cutter location and the material removal process [18]. Thus, for model-based active controllers, the model parameters are very hard to acquire online. 3) Unlike milling process, the plate is rotating during turning; and because of the limited space coupled with interference between the plate and the machine tool, it is very hard to capture the vibration displacement of thin plates at the cutting point. To the best of our knowledge, active chatter control in thin plate turning has seldom been studied.

This paper contributes to the development of an active control method, consisting of an adaptive sliding-mode controller (ASMC) and a displacement field reconstruction (DFR) method [19], for chatter suppression of thin plate by solving all three difficulties mentioned above. The ASMC, which does not rely on model parameters in implementation, is designed to suppress thin plate chatter actively during turning. In order to capture the dynamic behavior of the thin plate during turning, the DFR method reconstructs the vibration displacement of the plate at the cutting point for feedback control. Unlike existing control methods based on the lumped-parameter single-DOF cutting model, a distributed-parameter dynamic model of a rotating thin plate with multiple vibration modes is used to analyze the

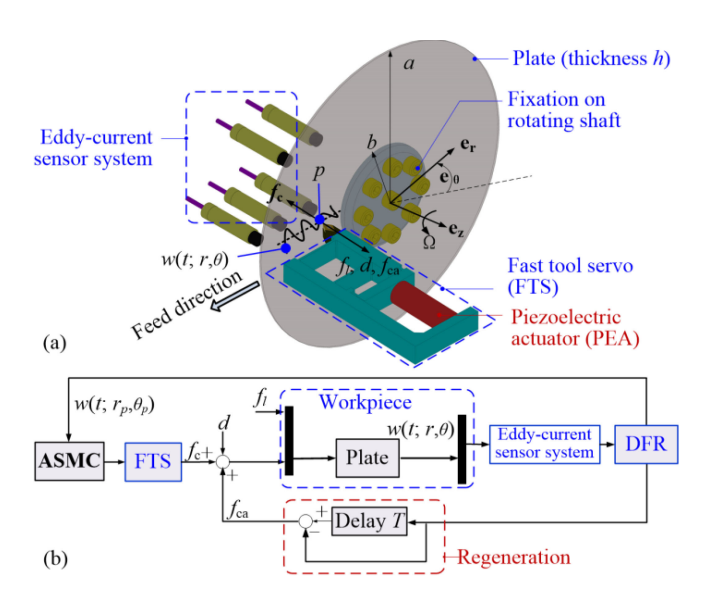


Fig. 1. Feedback control of lathe turning of a thin plate. (a) Lathe turning of a thin-walled plate. (b) Block diagram illustrating the active control method.

machining stability with the developed controller. A fast tool servo (FTS) is adopted as the execution unit of the developed method. Experimental results obtained on a lathe are presented to demonstrate the effectiveness of the active control method.

II. ACTIVE CONTROL METHOD FOR CHATTER SUPPRESSION

Fig. 1 schematically illustrates the active control method for lathe-turning of a thin plate clamped to a shaft rotating at the speed of Ω . As illustrated in Fig. 1(a), the WP being machined is an annular thin plate (outer radius a, inner radius b, thickness h, and elastic modulus E). Because the plate thickness h is very small compared with its radius ($h \ll a$), the dynamics of the plate that has the smallest stiffness in the normal direction of its mid-surface is dominant by the out-of-surface displacement $w(t; r, \theta)$ in polar coordinates $[r, \theta]$. Thus, the active control method for chatter suppression consists of two parts [Fig. 1(b)]: an ASMC designed to adapt to the time-varying system and the DFR [19] served as an observer to monitor the plate vibration in real time. The vibration displacement $w(t; r_p, \theta_p)$ is reconstructed from a set of eddy-current (EC) displacement sensors appropriately positioned around the plate, and is fed back to the ASMC that actively suppresses the plate vibration through a piezoelectric actuator (PEA) housed in the FTS.

A. Distributed-Parameter Model of the Thin Plate Dynamics

The WP is subjected to its own body centrifugal force f_l as well as disturbance d in addition to external loads that include the dynamic cutting force f_{ca} and active control force f_c .

Considering the oblique cutting model, the total dynamic cutting force can be expressed as [21]

$$\begin{cases} f_f \\ f_r \end{cases} = \frac{a_p}{\cos c} \begin{bmatrix} K_f \\ K_r \end{bmatrix} \left[\cos c - \sin c \right] \begin{Bmatrix} \Delta x \\ \Delta y \end{Bmatrix}$$
(1)

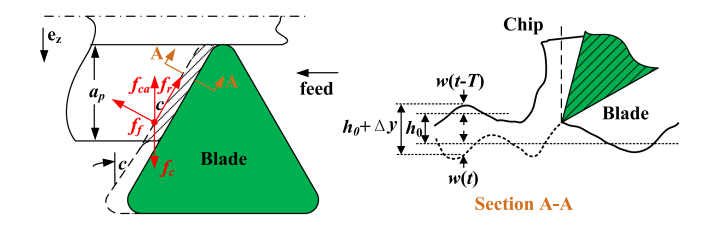


Fig. 2. Schematic representation of the chatter in turning process.

where f_f and f_r are the components of the total cutting force; a_p is the chip width; K_f and K_r are the corresponding cutting force coefficients; c is the side-edge cutting angle; Δx and Δy are the dynamic chip thickness. Considering Fig. 2, since the plate has the smallest stiffness in the normal direction of its mid-surface, the in-plane displacement Δx is negligible, $\Delta y = w(t-T; r_p, \theta_p) - w(t; r_p, \theta_p)$ and only consider the dynamic cutting force f_{ca} (normal to the mid-surface of plate). $T = 60/\Omega$ is the regenerative delay equivalent to a period of rotation. By coordinate transformation, and noting (1), f_{ca} can be expressed

$$\begin{split} &f_{ca}\left(t;r_{p},\theta_{p}\right) \\ &= \tan c\left\{K_{f}\sin c + K_{r}\cos c\right\}a_{p}\left[w\left(t - T;r_{p},\theta_{p}\right)\right. \\ &\left. - w\left(t;r_{p},\theta_{p}\right)\right]\delta\left((r - r_{p}),\left(\theta - \theta_{p}\right)\right) \\ &= K_{t}a_{p}\left[w\left(t - T;r_{p},\theta_{p}\right) - w\left(t;r_{p},\theta_{p}\right)\right]\delta\left((r - r_{p}),\left(\theta - \theta_{p}\right)\right) \end{split}$$

$$f_c(t; r_p, \theta_p) = u(t) \delta((r - r_p), (\theta - \theta_p)).$$
(2b)

In (2a), $K_t = \{K_f \sin c + K_r \cos c\} \tan c$. Since the dynamic cutting force f_{ca} is a point load, f_c is modeled with a spatial impulse $\delta()$ [22] at the cutting point $p(r_p, \theta_p)$ in (2b), where the u(t) is to be designed. f_c and f_{ca} are both perpendicular to the plate's mid-surface. The distributed state-variable $w(t; r, \theta)$ is governed by the dynamic model (3), where (\mathbf{m} and \mathbf{k}) are the elemental (inertias and elasticity) Laplacian operators and \mathbf{c} is a damping coefficient

$$\mathbf{m}\ddot{w}(t;r,\theta) + \mathbf{c}\dot{w}(t;r,\theta) + \mathbf{k}w(t;r,\theta) = f_l(t;r,\theta;\Omega) + f_{ca}(t;r,\theta) + f_c(t;r,\theta).$$
(3)

For completeness, the elemental Laplacian operators and the centrifugal force f_l are explicitly given in Appendix A.

Without loss of generality, the displacement field is expressed as a serial product of time and spatial components [23]

$$w(t; r, \theta) = \sum_{i=0}^{k} \phi_i(r, \theta) q_i(t)$$
 (4)

where ϕ_i is the *i*th mode shape determined by the inertia and stiffness as well as given boundary constraints; and q_i is the corresponding modal coordinates. Neglecting higher order terms, the displacement field is approximated by the lowest k orders in (4).

As detailed in Appendix B, substituting (4) into (3), the dynamic model of the distributed state variable $w(t; r, \theta)$ is reduced to (5a) characterized by a finite sets of mode shapes $\phi_i(r_p, \theta_p)$ and time-varying modal coordinates $q_i(t)$ where i = 0, 1, ..., k

$$\tilde{M}_i \ddot{q}_i(t) + \tilde{C}_i \dot{q}_i(t) + \tilde{K}_i q_i(t) = \phi_i(r_p, \theta_p) F_{ca} + \phi_i(r_p, \theta_p) u(t)$$
(5a)

$$\tilde{M}_{i} = \int_{0}^{2\pi} \int_{b}^{a} \rho h \phi_{i}^{2} r dr d\theta \tag{5b}$$

$$\tilde{C}_i = \int_0^{2\pi} \int_b^a \mu \phi_i^2 r dr d\theta \tag{5c}$$

$$\tilde{K}_{i} = \int_{0}^{2\pi} \int_{b}^{a} \phi_{i} \mathbf{k} \phi_{i} r dr d\theta \tag{5d}$$

and

 $F_{ca}(t)$

$$= -K_t a_p \left[\sum_{i=0}^k \phi_i(r_p, \theta_p) q_i(t) - \sum_{i=0}^k \phi_i(r_p, \theta_p) q_i(t-T) \right].$$
(5e)

In state-space representation with $\mathbf{q}(t) = [q_0 \dots q_i \dots q_k]^T$, (5a) can be recast into (6), where $\mathbf{d}(t)$ represents the combined effect of parameter uncertainties, external disturbance, and residual nonlinearity, including hysteresis and creep of PEA. The elements of the diagonal matrixes (\mathbf{M} , \mathbf{C} , \mathbf{K}) are given by (5b)–(5d)

$$\mathbf{M}\ddot{\mathbf{q}}(t) + \mathbf{C}\dot{\mathbf{q}}(t) + (\mathbf{K} + \bar{\mathbf{K}}_1)\mathbf{q}(t)$$
$$-\bar{\mathbf{K}}_1\mathbf{q}(t-T) + \mathbf{d}(t) = \mathbf{\Phi}u(t) \tag{6}$$

where

$$\mathbf{\Phi}(r_p, \theta_p) = \begin{bmatrix} \phi_0 \\ \phi_1 \\ \vdots \\ \phi_k \end{bmatrix} \text{ and } \frac{\mathbf{\bar{K}_1}(r_p, \theta_p)}{K_t a_p} = \begin{bmatrix} \phi_0^2 & \phi_0 \phi_1 & \cdots & \phi_0 \phi_k \\ \phi_1 \phi_0 & \phi_1^2 & \cdots & \phi_1 \phi_k \\ \vdots & \vdots & \ddots & \vdots \\ \phi_k \phi_0 & \phi_k \phi_1 & \cdots & \phi_k^2 \end{bmatrix}.$$

The above formulation reduces the partial differential (3) with infinite-DOFs to an uncoupled kth-order ordinary differential (6), where the displacement field $w(t; r, \theta)$ has been transformed into a finite set of modal coordinates $\mathbf{q}(t)$ to facilitate the controller design.

B. Adaptive Controller Design

Noting (4), the sliding function is defined in (7) where c_1 is a positive constant

$$s(t) = c_1 \sum_{i=0}^{k} \phi_i(r_p, \theta_p) q_i(t) + \sum_{i=0}^{k} \phi_i(r_p, \theta_p) \dot{q}_i(t).$$
 (7)

Next, an ASMC is designed to force the system states to reach the neighborhood of the sliding surface with Assumption 1. Assumption 1: Disturbance $\mathbf{d}(t)$ is bounded and satisfies (8) where k_1 (>0) is the unknown bound of the total disturbance

$$\left|\mathbf{\Phi}^T \mathbf{M}^{-1} \mathbf{d}(t)\right| \le k_1 \left\|\psi\right\| \tag{8a}$$

where

$$\mathbf{\psi}(t) = \begin{bmatrix} \mathbf{q}^T \ \dot{\mathbf{q}}^T \ 1 \end{bmatrix}. \tag{8b}$$

Lemma 1: The model parameters of the thin plate and system states satisfy inequality (9) where k_4 is the unknown bound of the model parameters and disturbance [24]

$$\left| (c_1 \mathbf{\Phi}^T - \mathbf{\Phi}^T \mathbf{M}^{-1} \mathbf{C}) \dot{\mathbf{q}}(t) \right|$$

$$+ \left| \mathbf{\Phi}^T \mathbf{M}^{-1} (\mathbf{K} + \bar{\mathbf{K}}_1) \mathbf{q}(t) \right| < (k_4 - k_1) \| \psi \| .$$
 (9)

Proof: The left side of (9) can be written into the following two inequalities:

$$\left| (c_1 \mathbf{\Phi}^T - \mathbf{\Phi}^T \mathbf{M}^{-1} \mathbf{C}) \dot{\mathbf{q}}(t) \right| \le \left\| c_1 \mathbf{\Phi}^T - \mathbf{\Phi}^T \mathbf{M}^{-1} \mathbf{C} \right\| \left\| \dot{\mathbf{q}}(t) \right\|$$
(10a)

$$\left| \mathbf{\Phi}^T \mathbf{M}^{-1} (\mathbf{K} + \bar{\mathbf{K}}_1) \mathbf{q}(t) \right| \le \left\| \mathbf{\Phi}^T \mathbf{M}^{-1} (\mathbf{K} + \bar{\mathbf{K}}_1) \right\| \| \mathbf{q}(t) \|$$
(10b)

Let
$$\mathbf{\Xi}_1 = c_1 \mathbf{\Phi}^T - \mathbf{\Phi}^T \mathbf{M}^{-1} \mathbf{C} = \begin{bmatrix} \gamma_{10} \ \gamma_{11} \cdots \ \gamma_{1k} \end{bmatrix}$$
 (11a)

$$\Xi_2 = \mathbf{\Phi}^T \mathbf{M}^{-1} (\mathbf{K} + \bar{\mathbf{K}}_1) = \left[\gamma_{20} \ \gamma_{21} \cdots \ \gamma_{2k} \right]. \tag{11b}$$

Noting that
$$|\Xi_1 \dot{\mathbf{q}}(t)| \le ||\Xi_1|| ||\dot{\mathbf{q}}(t)||$$
 (12a)

$$|\Xi_2 \mathbf{q}(t)| \le \|\Xi_2\| \|\mathbf{q}(t)\|.$$
 (12b)

The positive constant k_4 which satisfies the condition $(k_4 - k_1) > 2 \times \max\{||\Xi_1||, ||\Xi_2||\}$ can be found since $||\Xi_1||$ and $||\Xi_2||$ are bounded and (13a) and (13b) are always held

$$\|\dot{\mathbf{q}}(t)\| < \|\psi\| = \sqrt{\|\dot{\mathbf{q}}(t)\|^2 + \|\mathbf{q}(t)\|^2 + 1}$$
 (13a)

$$\|\mathbf{q}(t)\| < \|\psi\| = \sqrt{\|\dot{\mathbf{q}}(t)\|^2 + \|\mathbf{q}(t)\|^2 + 1}.$$
 (13b)

Based on the analysis, it is deduced that inequality (9) can be satisfied. This conclusion will be used later in Theorem 1.

Remark 1: It should be noted that Lemma 1 is satisfied for the thin plate turning system, since there always exists damping in flexible structures. Even small damping ensures that the magnitude of vibration is bounded.

Remark 2: Since various disturbances exist in machining in addition to the fact that the model parameters of the thin plate vary with material removal and cutter location, an accurate knowledge of the bound k_4 cannot be easily obtained. In order to relax the bound on the system parameters and disturbances, an adaptive control method is necessary to estimate the bound in the sense of Lyapunov [25].

Thus, ASMC is designed as

$$u(t) = -\frac{\tau s_0}{s_0 + |s(t)|} s(t) - \left[\delta \hat{\eta} \hat{k} \|\psi\| + \hat{\varsigma} \|\mathbf{q}(t - T)\| \right] \frac{s(t)}{|s(t)|}$$
(14a)

with $\delta > 1$ and $p_1 > 0$

$$\hat{k} = p_1 |s(t)| \|\psi\|$$
 (14b)

$$\dot{\hat{\eta}} = \delta \hat{\eta}^3 \hat{k} |s(t)| \|\psi\| \tag{14c}$$

$$\dot{\hat{\varsigma}} = |s(t)| \|\mathbf{q}(t-T)\|.$$
 (14d)

In (14a), the first term employs the sliding function to form the nonswitching reaching law [20] to increase the convergence rate and alleviate chattering of the SMC. The second term uses the sliding function to construct the switching function, s(t)/|s(t)|.

Remark 3: The nonswitching reaching law [20] is adopted here. By properly tuning the parameters τ and s_0 , the system convergence to the neighborhood of the sliding surface will be speeded up; and the undesired chatter (that is a disadvantage of the SMC [25]) can be reduced simultaneously [20].

Remark 4: The unknown bound k_4 is estimated by the adaptive law \hat{k} [26]; and the initial value $\hat{k}(0) > 0$ must be selected to guarantee $\hat{k}(t) > 0$ $\hat{k}(t)$ for $\forall t \in [0 \infty)$. The adaptive laws $\hat{\eta}$ and $\hat{\varsigma}$ are constructed to tackle the unknown model parameters and regenerative delay term [3].

The effectiveness of chatter suppression is guaranteed by the following stability of the designed controller.

Theorem 1: For system (6) with Assumption 1 and the designed controller (14a)–(14d) under condition (9), the suppression of the chatter in the turning process can be guaranteed by driving the system states asymptotically from any initial state to the neighborhood of the sliding surface and maintaining the bounded system states.

Proof: Consider the following Lyapunov function (15a) in terms of the estimation errors $(\tilde{k}, \tilde{\eta}, \text{ and } \tilde{\varsigma})$ [14]:

$$V_{sa} = \frac{1}{2} \left[s^2(t) + \frac{1}{p_1} \tilde{k}^2 + \tilde{\eta}^2 + \Gamma \tilde{\varsigma}^2 \right]$$
 (15a)

where

$$\Gamma = \mathbf{\Phi}^T \mathbf{M}^{-1} \mathbf{\Phi} \tag{15b}$$

and

$$\varsigma = \mathbf{\Phi}^T \mathbf{M}^{-1} \bar{\mathbf{K}}_1 \tag{15c}$$

$$\tilde{k} = k_4 - \hat{k}, \tilde{\eta} = \Gamma - \hat{\eta}^{-1} \tag{15d}$$

and

$$\tilde{\varsigma} = \Gamma^{-1} \|\varsigma\| - \hat{\varsigma}. \tag{15e}$$

The time-derivative of the Lyapunov function is given by

$$\dot{V}_{sa} = s(t)\dot{s}(t) - \frac{\left(\tilde{k}\dot{k}\right)}{p_1} + \tilde{\eta}\hat{\eta}^{-2}\dot{\hat{\eta}} + \left(\Gamma\hat{\varsigma} - \|\varsigma\|\right)\dot{\hat{\varsigma}}$$
 (16a)

where

$$\dot{s}(t) = c_1 \mathbf{\Phi}^T \dot{\mathbf{q}}(t) + \mathbf{\Phi}^T \ddot{\mathbf{q}}(t) \text{ from (7)}. \tag{16b}$$

With some algebra operations, (6) can be written as

$$\mathbf{\Phi}^{T}\ddot{\mathbf{q}}(t) = -\mathbf{\Phi}^{T}\mathbf{M}^{-1}\mathbf{C}\dot{\mathbf{q}}(t) - \mathbf{\Phi}^{T}\mathbf{M}^{-1}(\mathbf{K} + \bar{\mathbf{K}}_{1})\mathbf{q}(t) + \mathbf{\Phi}^{T}\mathbf{M}^{-1}\bar{\mathbf{K}}_{1}\mathbf{q}(t-T) - \mathbf{\Phi}^{T}\mathbf{M}^{-1}\mathbf{d}(t) + \mathbf{\Phi}^{T}\mathbf{M}^{-1}\mathbf{\Phi}u(t).$$
(17)

Substitute (17) and (15c) into (16b)

$$\dot{s}(t) = \left(c_1 \mathbf{\Phi}^T - \mathbf{\Phi}^T \mathbf{M}^{-1} \mathbf{C}\right) \dot{\mathbf{q}}(t) - \mathbf{\Phi}^T \mathbf{M}^{-1} (\mathbf{K} + \mathbf{\bar{K}_1}) \mathbf{q}(t)$$
$$+ \varsigma \mathbf{q}(t - T) - \mathbf{\Phi}^T \mathbf{M}^{-1} \mathbf{d}(t) + \mathbf{\Phi}^T \mathbf{M}^{-1} \mathbf{\Phi} u(t)$$

and noting Assumption 1, $s(t)\dot{s}(t) \leq |s(t)||(c_1\boldsymbol{\Phi}^T - \boldsymbol{\Phi}^T \mathbf{M}^{-1}\mathbf{C})\dot{\mathbf{q}}(t)| + |s(t)||\boldsymbol{\Phi}^T \mathbf{M}^{-1}(\mathbf{K} + \bar{\mathbf{K}}_1)\mathbf{q}(t)| + s(t)\varsigma\mathbf{q}(t - T) + k_1|s(t)||\psi|| + s(t)\boldsymbol{\Phi}^T \mathbf{M}^{-1}\boldsymbol{\Phi}u(t).$

After accounting for Lemma 1, the first term in (16a) satisfies (18a) where u(t) is defined in (14a)

$$s(t)\dot{s}(t) \le (k_4 - k_1) |s(t)| ||\psi|| + s(t)\varsigma \mathbf{q}(t - T)$$

+ $k_1 |s(t)| ||\psi|| + s(t)\mathbf{\Phi}^T \mathbf{M}^{-1}\mathbf{\Phi}u(t).$ (18a)

From (14b), the second term of (16a) can be written as

$$\left(\tilde{k}\hat{k}\right)/p_1 = \tilde{k}\left|s(t)\right| \|\psi\|. \tag{18b}$$

From (14c) and (15b), the third term can be rewritten as

$$\tilde{\eta}\hat{\eta}^{-2}\dot{\hat{\eta}} = \delta\left(\mathbf{\Phi}^T\mathbf{M}^{-1}\mathbf{\Phi}\hat{\eta} - 1\right)\hat{k}\left|s(t)\right|\left\|\psi\right\|. \tag{18c}$$

With (15b) and (14d), the fourth term in (16a) becomes

$$(\Gamma \hat{\varsigma} - \|\varsigma\|) \dot{\hat{\varsigma}} = \left[\left(\mathbf{\Phi}^T \mathbf{M}^{-1} \mathbf{\Phi} \right) \hat{\varsigma} - \|\varsigma\| \right] |s(t)| \|\mathbf{q}(t - T)\|.$$
(18d)

Substituting (18a)–(d), along with (14a), into (16a) leads to

$$\dot{V}_{sa} \le (1 - \delta)\hat{k} |s(t)| \|\psi\| - \mathbf{\Phi}^{\mathrm{T}} \mathbf{M}^{-1} \mathbf{\Phi} \left[\frac{\tau s_o}{s_o + |s(t)|} \right] s^2(t)$$

$$\tag{19}$$

where $\Phi^T M^{-1}\Phi = \sum_{i=0}^k \phi_i^2 \ (r_p,\theta_p) M_i^{-1} \ge 0$. From (14b) where $p_1 > 0$, it is deduced that $\hat{k} > 0$ provided $\hat{k}(0) > 0$. Hence, $\dot{V}_{sa} < 0$ can be guaranteed with $\delta > 1$ for all $s(t) \ne 0$. The states of closed-loop system are bounded, implying that the chatter is suppressed. This completes the proof of Theorem 1.

Remark 5: The controller parameters can be obtained by trial-and-error method. More specifically, the parameter selection falls into three steps: i) First, the parameters δ (>1) and p_1 (>0) of adaptive laws \hat{k} , $\hat{\eta}$ [(14b) and (14c)] should be adjusted to guarantee a stable turning process. To speed up the convergence rates of \hat{k} and $\hat{\eta}$ to the desired ones, large δ and p_1 should be selected. For example, the adjustment of parameter δ can be carried out by setting other parameters as 0.1. By this means, it is convenient to determine an appropriate value for δ because only this parameter is tuned. It should be noted that too large δ will cause performance deterioration and even system instability. In practice, the parameter δ is assigned by making a tradeoff. ii) Then, the parameter τ in (14a) [20] and the parameter c_1 in (7) are tuned to speed up the system convergence to the neighborhood of the sliding surface. However, the undesired chattering, which is one of the disadvantages of the SMC, will enlarge by increasing τ and c_1 . iii) Finally, the reaching law parameter s_0 in (14a) [20] is tuned to reduce the undesired chattering. A tradeoff is made between the system convergence, i.e., speed of chatter suppression and the amplitude of undesired chattering.

C. Displacement Field Reconstruction

Since plate vibration at the cutting point is difficult to measure, the DFR is employed to reconstruct $w(t; r_p, \theta_p)$ and $\mathbf{q}(t)$ for displacement feedback of the designed ASMC. The hardware configuration of DFR is illustrated in Fig. 1(a). According to (4) and [19], [23], the displacement field is rewritten as

$$w(t; r, \theta) = \sum_{i=0}^{k} \left[\alpha_i(t) \phi_i^C(r, \theta) + \beta_i(t) \phi_i^S(r, \theta) \right]$$
 (20)

where α_i and β_i are the time-varying coefficients; and the mode shapes $\phi_i^C(r,\theta) = \phi_i(r)\cos(i\theta)$ and $\phi_i^S(r,\theta) = \phi_i(r)\sin(i\theta)$.

Consider N EC displacement sensors positioned around the plate to monitor w at $\mathbf{R}_n = (r_n, \theta_n)$ where n = 1, 2, ..., N.

In matrix form (21a) where $\mathbf{a} = [\boldsymbol{\alpha} \, \boldsymbol{\beta}]^T$, the coefficients in (20), $\boldsymbol{\alpha} = [\alpha_0 \dots \alpha_k]^T$ and $\boldsymbol{\beta} = [\beta_0 \dots \beta_k]^T$, can be calculated in terms of the measurements **W** and mode shapes $\mathbf{S} = [\mathbf{S}_C \, \mathbf{S}_S]$

$$\mathbf{a} = (\mathbf{S}^{\mathsf{T}}\mathbf{S})^{-1}\mathbf{S}^{\mathsf{T}}\mathbf{W} \tag{21a}$$

where

$$\mathbf{W} = \left[w(t; \mathbf{R}_1) \cdots w(t; \mathbf{R}_N) \right]^T$$
 (21b)

and
$$\mathbf{S}_{j=\text{Cor }S} = \begin{bmatrix} \phi_0^j(\mathbf{R}_1) \dots & \phi_i^j(\mathbf{R}_1) & \dots & \phi_k^j(\mathbf{R}_1) \\ \phi_0^j(\mathbf{R}_2) \dots & \phi_i^j(\mathbf{R}_2) & \dots & \phi_k^j(\mathbf{R}_2) \\ \vdots & \vdots & \ddots & \vdots \\ \phi_0^j(\mathbf{R}_N) \dots & \phi_i^j(\mathbf{R}_N) & \dots & \phi_k^j(\mathbf{R}_N) \end{bmatrix}.$$

$$(21c)$$

In (21c), the subscript "j" in \mathbf{S}_j and superscript "j" in ϕ_i^j denote C or S in the mode shapes in (20), $\phi_i^C(r,\theta)$ or $\phi_i^S(r,\theta)$. In view of (21a \sim c), there are N known quantities and (2k+2) unknown quantities. The mode shapes, $\phi_i^C(r,\theta)$ and $\phi_i^S(r,\theta)$, can be obtained by offline computing and only the modal coefficients require online calculating by solving the linear equation (21a)–(21c). Hence, DFR has high computing efficiency and this method is suitable for real-time application.

The reconstruction accuracy of DFR is affected by the sensor locations (radius and angle), number of sensors (modes), and the measurement noise. For the sensor locations, through the genetic algorithm in the MATLAB Optimization Toolbox, the sensor locations are optimized by finding a proper matrix S that minimizes the condition number $\operatorname{cond}(S)$ (= $\|S\|\cdot\|S^{-1}\|$). Considering Fig. 1(a), the EC sensors are positioned close to the spindle motor, the measurement signals may be noisy, and hence the LMS (least mean square) filter in the MATLAB Filtering Toolbox is used to smooth them. Moreover, more sensors and modes lead to higher reconstruction accuracy. However, this will result in a larger modal coefficient matrix and thus longer calculation time. Hence, tradeoffs should be made between the number of sensors (modes) and the reconstruction efficiency in terms of reconstruction accuracy and computation time.

Based on the formulation in Section II, the active control method can be implemented with the aid of the flowchart in Fig. 3. For specific applications, $\phi_i^C(r,\theta)$ and $\phi_i^S(r,\theta)$ can be

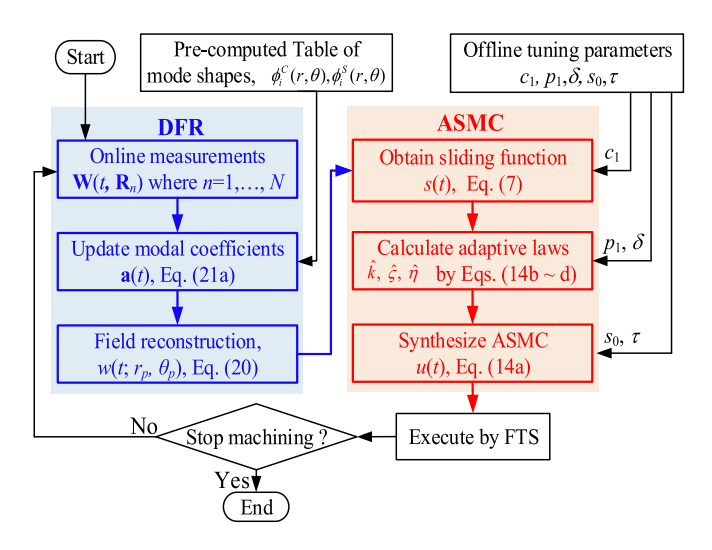
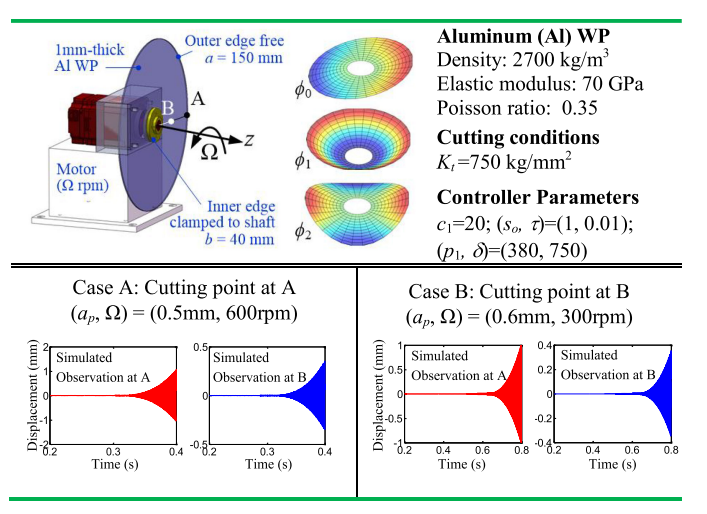


Fig. 3. Flowchart illustrating the active control method.

TABLE I PARAMETRIC VALUES USED IN SIMULATION



precomputed/stored as a look-up table; and the control parameters $(c_1, p_1, \delta, s_0, \text{ and } \tau)$ can be tuned offline. The DFR reconstructs the w field from online measurements, from which the WP displacement $w(t; r_p, \theta_p)$ at the cutting point is fedback to the ASMC as illustrated in Fig. 3, where the coefficients $\mathbf{a}(t)$ and modal coordinates $\mathbf{q}(t)$ are equivalent.

D. Numerical Illustration and Verification

The effectiveness of the active control method for chatter suppression is numerically illustrated using published parametric values [19], [23] for the setup shown in Table I (left of top row). The DFR [19], [23] is used to reconstruct the vibration displacement at specified points of the plate.

As illustrated in Table I, three mode shapes ϕ_0 , ϕ_1 , and ϕ_2 are used in the DFR in this investigation. For visualization, the displacements at points A and B (along $\theta=0^\circ$ at the edge and mid-radius, respectively) simulated using (4) subject to a cutting force exerted at point A or B (referred to here as Case A and

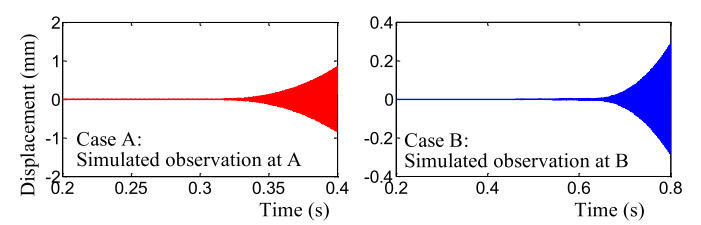


Fig. 4. Simulations illustrating the active damping [9], [10] performance.

Case B, respectively) are displayed in the bottom row of Table I. In both cases (with different widths-of-cut a_p and spindle speeds Ω), the WP displacements of the uncontrolled system diverge.

It is worth noting that the tuneable vibration absorber (TVA) in [17] cannot be applied to this situation because it was designed for chatter mitigation of boring bars. The TVA has to maintain contact with the controlled objects; this is impossible for the chatter suppression in thin plate turning as the WP rotates and will interfere with the TVA. The model-based active controllers, like [4]–[13], are also very hard to accommodate this situation because the WP considered here is a spatially distributed system and its parameters (mass, stiffness, and damping) vary greatly with the changing of cutter location. The active damping method with direct velocity feedback [9], [10] does not require a very accurate model of the controlled objects; for comparison purposes, it is employed here using the same input as the ASMC. As seen in Fig. 4, the WP cannot be stable for both cases, no matter how the active damping method tunes its control parameters.

The simulated displacements under the sliding-mode control are numerically demonstrated in Figs. 5–7. Fig. 5 shows the vibration displacement of the WP (as observed at A and B) converges to a steady state (defined by a residual vibration tolerance of 1 μ m) within 1.35 s for Case A (left column) and 2.52 s for Case B (right column), demonstrating that the chatter can be effectively suppressed within tolerance under the sliding-mode control. As shown in Fig. 5 where the sliding functions (third row) and control forces (fourth row) are plotted, the sliding states are driven onto and maintained in the neighborhood of the sliding surface, and thus the sliding modes are stable.

To suppress chatter, five parameters $[c_1, (s_0, \tau)]$, and (p_1, δ)] of the ASMC are numerically tuned based on Remarks 3 and 5 to achieve a satisfactory convergence rate and control performance for a range of rotational speeds Ω and width-of-cut a_p . The parameters $(c_1 \text{ and } \tau)$ are selected to rapidly suppress chatter as depicted in Fig. 6(a) where s_0 is tuned to reduce the undesired chattering of sliding-mode control; and (p_1, δ) are in relation to the amplitude of chatter as shown in Fig. 6(b).

Fig. 7 shows the results, numerically illustrating the control performance of the designed controller. Unlike the simulation in Fig. 5 where the control action is exerted from the beginning, the control action in the simulation summarized in Fig. 7 is exerted from 0.35 s (representing a more rigorous working condition since severe chatters have already lasted for 0.35 s). In this paper, the cutting (with a width-of-cut $a_p=0.9\,\mathrm{mm}$) is assumed to be exerted at point A while the WP rotates at $\Omega=600\,\mathrm{rpm}$.

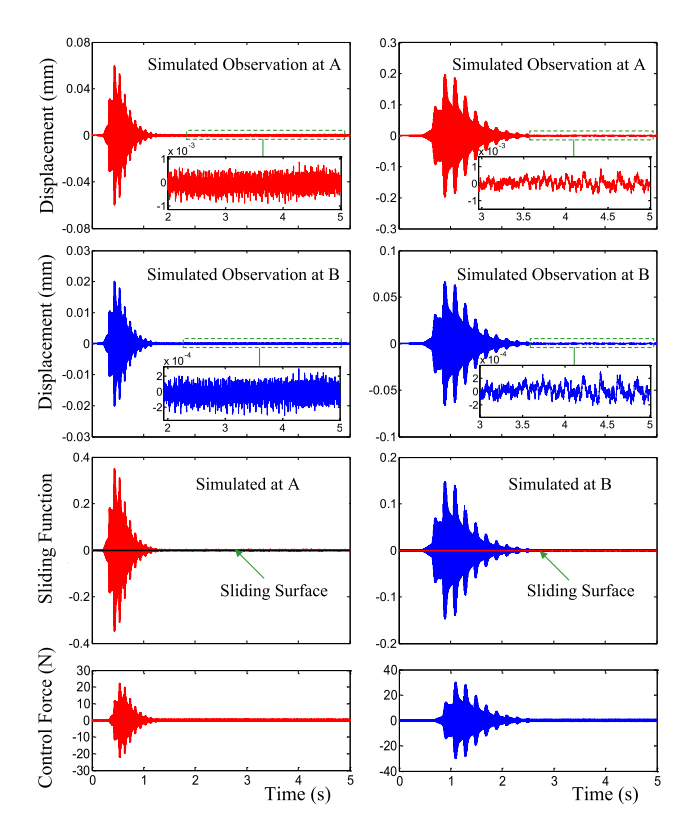


Fig. 5. Typical simulated ASMC performances. Left: Case A. Right: Case B.

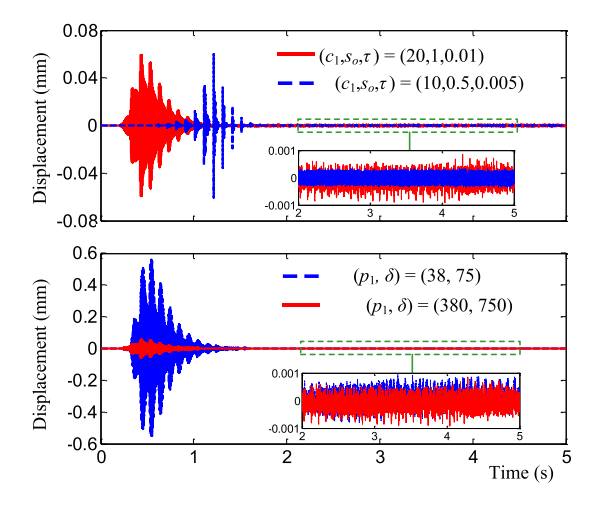


Fig. 6. ASMC performance. Top: Effects of (c_1, s_0, τ) . Bottom: Effects of (p_1, δ) .

Using the same controller parametric values in Table I but switching on at 0.35 s when chatter has already occurred, the effective attenuation of the chatter confirms that the designed controller will remain valid under different situations.

III. EXPERIMENTAL RESULTS AND DISCUSSION

The active control method for chatter suppression during turning of a thin plate has been experimentally evaluated using the

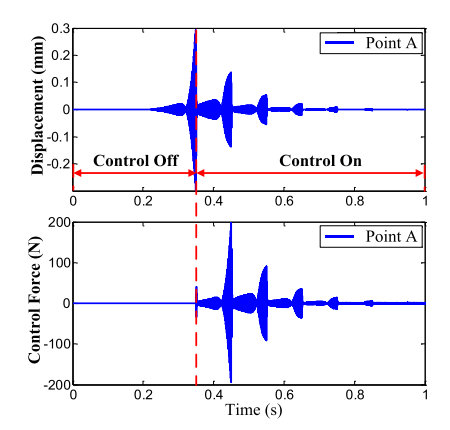


Fig. 7. Time response of the controlled plate at point A; cutting point A.

setup shown in Fig. 8, where results obtained from a conventional lathe turning without feedback control provide a basis for comparison.

During experiments, the thin annular (Aluminum 6061) plate was clamped at its inner edge on the shaft of a servomotor (Yaskawa SGMJV-08 ADE 6S with power 750 W, nominal torque 2.39 N m, and maximum torque 8.36 Nm). The free outer edge of the plate was passively damped by a pair of repulsion magnets to keep the vibration within the controllable range of the PEA-actuated FTS, where the stroke of PEA was amplified by the flexible-based mechanism (FBM). The PEA nonlinear hysteresis was compensated by the modified Prandtl–Ishlinskii model [27]. The inner and outer radii of the 2-mm-thick plate are 40 mm and 150 mm respectively, between which the annular region (69 mm $\leq r \leq$ 99 mm) is used for turning experiments [Fig. 8(b)].

Conducted on the testbed designed for duplex lathe turning of a thin WP [23], a pair of symmetrical cutters was applied on both sides of the WP to reduce deformation as well as to increase the stability margin of the cutting process. For clarity in illustrating the experimental verification with EC sensors on one side of the WP, only one cutter is applied (on the other side of the WP). During experiments, three mode shapes ϕ_0 , ϕ_1 , and ϕ_2 are used in the DFR. According to Section II-C, at least six EC sensors should be used for the DFR. However, since modal shape ϕ_0 is symmetric and has one coefficient α_0 , six EC sensors (with resolution of 0.1 μ m) are mounted in fixed locations to measure the WP vibration, as shown in Fig. 8(d); five of these sensors are employed for the DFR [19] and the first sensor provides a mean to evaluate the accuracy of the DFR. The output voltages of these sensors are simultaneously acquired by the analog-to-digital (A/D) converters with a sampling frequency of 3.3 kHz. The hardware specifications are listed in Table II.

Fig. 9 compares the WP displacement reconstructed from the five EC sensors using the DFR during turning with that measured directly by the first EC sensor. As shown in the zoomin plots, the DFR faithfully tracks the WP dynamics, and thus the reconstructed displacement at the cutting point is employed for subsequent feedback control. As mentioned before, the DFR has high computing efficiency.

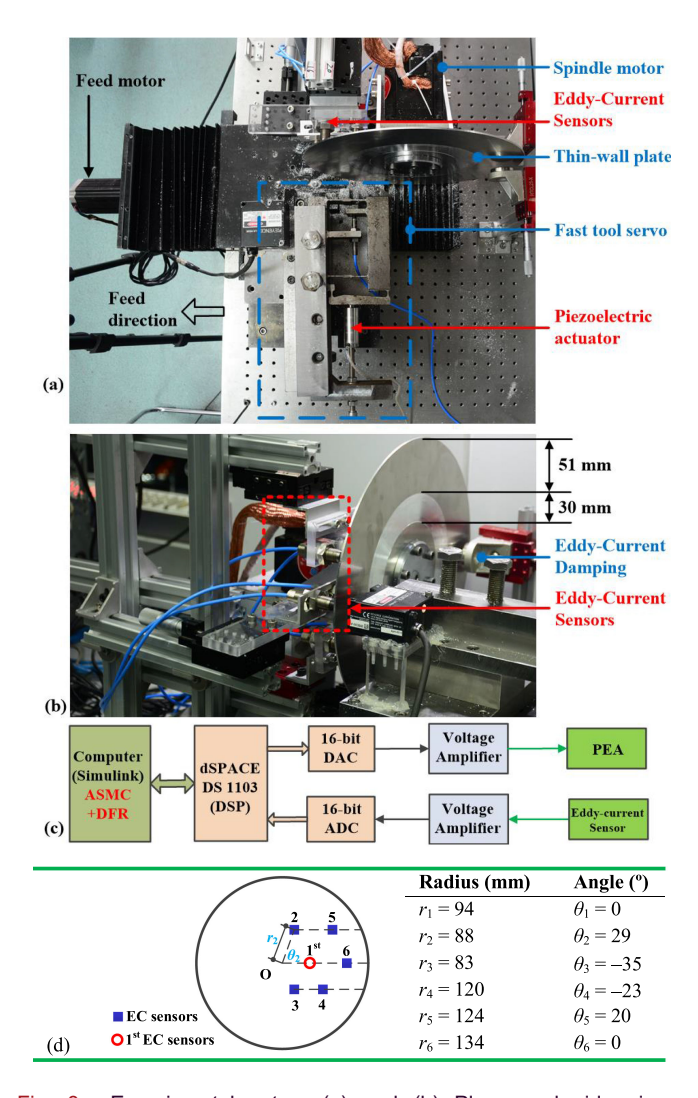


Fig. 8. Experimental setup. (a) and (b) Plane and side views. (c) Data acquisition and controller. (d) Configuration of eddy-current (EC) sensors.

ASMC with DFR the are programmed MATLAB/Simulink and downloaded via the ControlDesk interface to the dSPACE-DS1103 controller board equipped with 16-bit analog- to-digital (A/D) converters and 16-bit digitalto-analog (D/A) converters. The output signals of D/A converter are amplified for driving the piezoelectric actuator (PSt150/14/40VS20). The cutting conditions and ASMC parametric values are listed in Table III. Considering Remarks 3 and 5, the ASMC parameters are tuned by trial-and-error before the turning experiments. To speed up the convergence rates of kand $\hat{\eta}$ to the desired ones, large δ and p_1 should be selected. We can increase the values of parameters δ and p_1 gradually with a small step 0.05. However, too large δ and p_1 will make the FTS unstable (oscillatory response along with unwanted noise). Hence, the parameters δ and p_1 are assigned by making a tradeoff.

Four different cutting parameters are adopted in experiments: Comparison 1: $h_o=12.5~\mu\text{m/r}$, $a_p=40~\mu\text{m}$, $\Omega=600~\text{rpm}$. Comparison 2: $h_o=12.5~\mu\text{m/r}$, $a_p=50~\mu\text{m}$, $\Omega=550~\text{rpm}$. Comparison 3: $h_o=14.0~\mu\text{m/r}$, $a_p=35~\mu\text{m}$, $\Omega=500~\text{rpm}$. Comparison 4: $h_o=11.0~\mu\text{m/r}$, $a_p=40~\mu\text{m}$, $\Omega=600~\text{rpm}$.

TABLE II
SPECIFICATIONS OF HARDWARE

Eddy-current Sensor (CWY-DO-20XLT08-M10)			
Parameters	Performance		
Diameter (mm) 8	Response (kHz) 10		
Standoff (mm) 0.5	Range (mm) 2		
Input (Vdc) -24	Resolution (µm) 0.1		
Output (Vdc) -18 to -2	Linearity (\pm %FS) 1		
	Temp. stability (%FSR/°C) 0.04		
PEA (PSt150/14/40VS20)			
Parameters	Performance		
Diameter (mm) 20	Stroke (µm) 38		
Length (mm) 53	Push/pull force (N) 4700/700		
Input (V) -30 to 150	Resonance frequency (kHz) 20		
FTS amplification ratio 1 to 3 Stiffness $(N/\mu m)$ 120			

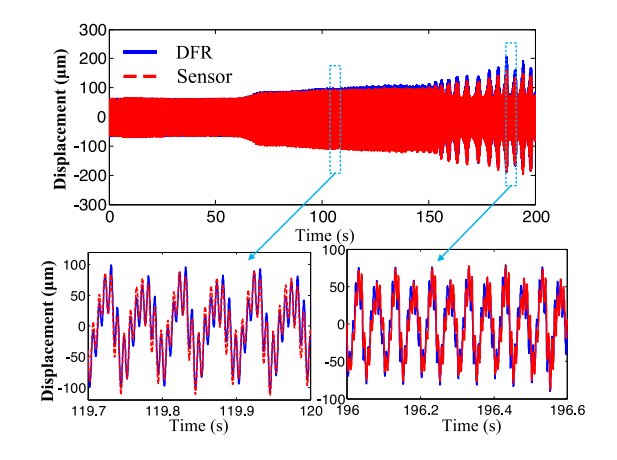


Fig. 9. Comparison between reconstructed and measured data.

TABLE III
CUTTING CONDITIONS AND CONTROLLER PARAMETERS

Cutting Conditions		Controller Parameters	
Blade	DCGT11T304	c_1	2
Cutter holder	SDJCR2020-K11	s_0	0.3
Feed rate, h_o (mm/r)	0.0125	τ	0.015
Width of cut, a_p (mm)	0.04/0.05	δ	1.5
Spindle speed, Ω (rpm)	600/550	p_1	1.3

In all four Comparisons, the chatters were effectively suppressed by the active ASMC-DFR control method. For conciseness and readability while avoiding repetitions, only the evaluation results for Comparisons 1 and 2, which are organized into two groups, are presented here.

The *first* group investigates the effects of the active control method on chatter suppression by comparing with convectional cutter without control under Comparison 1 (Fig. 10) and Comparison 2 (Fig. 11) where the estimated \hat{k} value is depicted in Fig. 11(b). To protect the PEA, an upper limit was imposed as an upper bound on \hat{k} in all the active control experiments. The WP vibration displacements at the cutting point are analyzed in Figs. 10(a) and 11(a) with surface finishes compared in Figs. 10(c) and (d) and 11(c) and (d).

The *second* group compares the active control method with the PID control (with the same reconstructed displacement at the cutting point from the DFR as input), where the PID parameters (i.e., $k_p = 0.6$, $k_i = 3$, $k_d = 0.001$) were

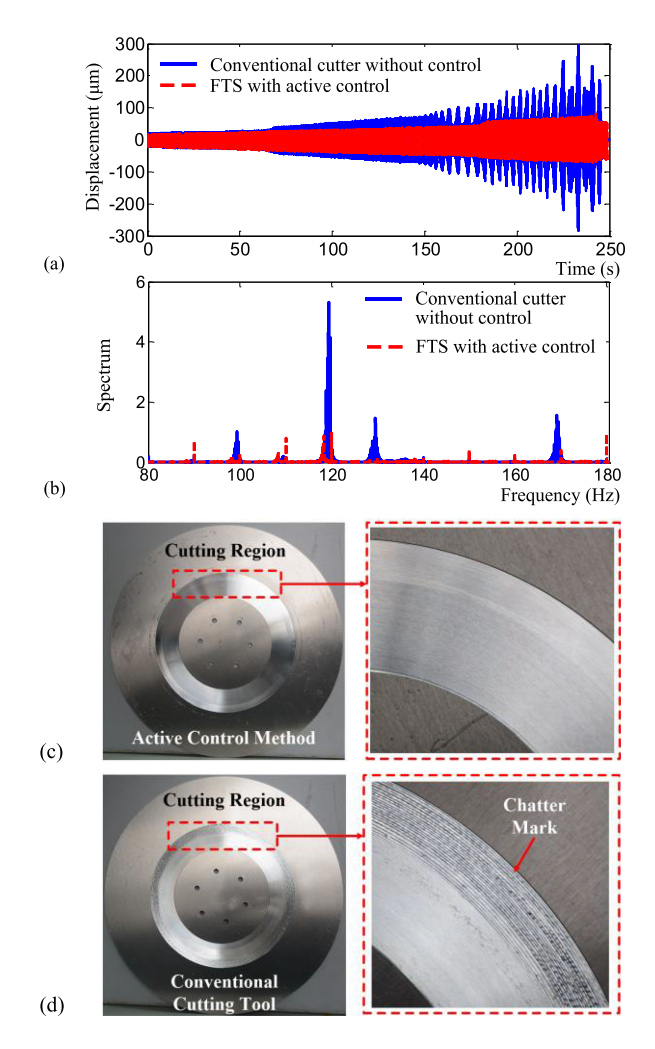


Fig. 10. Comparison 1. (a) Vibration displacement at cutting point. (b) FFT. (c) Plate surface under active control. (d) Plate surface by conventional tool.

tuned by trial-and-error before the turning experiments. The WP vibration displacements at the cutting point are compared in Fig. 12(a) (Comparison 1) and Fig. 12(b) (Comparison 2), along with the surface finishes under the PID for completeness.

From the experimental results presented in Figs. 10–12, the following observations can be made.

As compared in Figs. 10(a) and 11(a) under Comparisons 1 and 2, respectively, unlike the conventional cutter without control where chatter vibration grows incrementally in machining, the active control method with DFR maintains the WP vibration well within $\pm 70~\mu m$. However, chatter cannot be completely suppressed experimentally (different from the theoretical results in Section II-D); the reason is that controller parameters in the experiment cannot be adjusted large enough due to the presence of noise and external disturbance. The FTS, including the FBM and the PEA, causes phase lag of the control command. The control command cannot be perfectly executed by FTS as theoretical results in Section II-D due to the dynamics of FTS and residual nonlinearity in PEA.

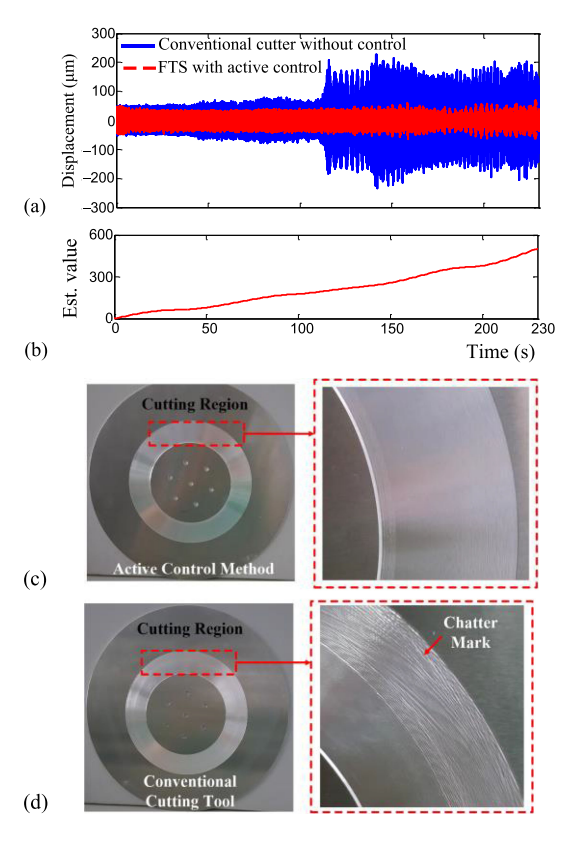


Fig. 11. Comparison 2. (a) Vibration displacement at cutting point. (b) Estimated value of \hat{k} . (c) Plate surface under active control. (d) Plate surface by conventional tool.

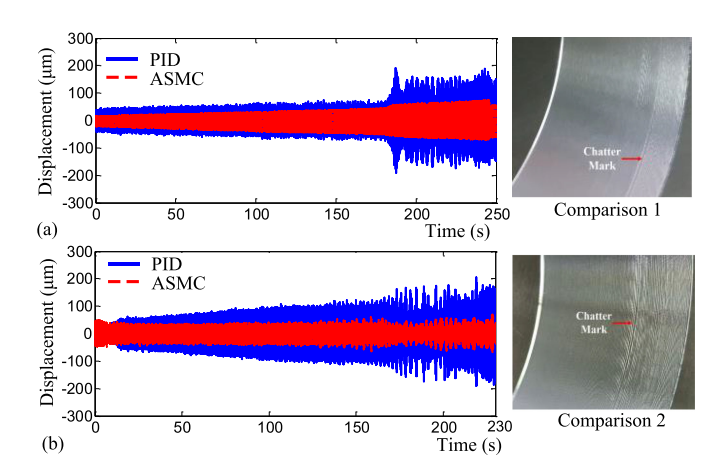


Fig. 12. PID controlled vibration displacement at cutting point and plate surface. (a) Comparison 1. (b) Comparison 2.

As shown in Figs. 10(a) and 11(a), the amplitudes of stable vibrations are considerable. Chatters are effectively suppressed with the proposed active control method; as a result, the WP vibrations are kept within the stable cutting region. The developed method achieves smoother surface finish with finer vibration marks than conventional cutter, as depicted in Figs. 10(c) and (d) and 11(c) and (d).

Fig. 10(b) compares the spectrum analyses of displacement measurements at the cutting point with/without active control.

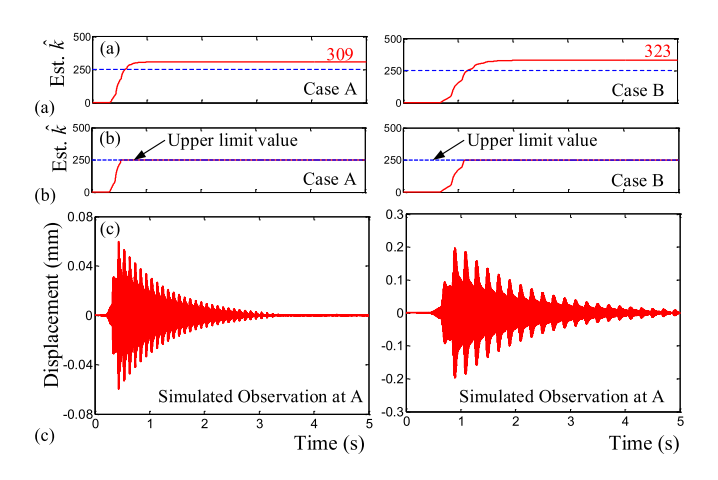


Fig. 13. Effects of imposing an upper \hat{k} limit on the active control. (a) Without upper limit on \hat{k} . (b) With upper limit on \hat{k} . (c) Vibration displacement at cutting point. Left column: Case A. Right column: Case B.

Without control, chatter vibration results in several peaks at multiple frequencies and their harmonics. It is worth noting that multiple modes of the thin plate can be easily excited; the first three natural frequencies of the plate are 115.6, 116.8, and 168.3 Hz. As observed from Fig. 10(b)–(d) and Fig. 11(c) and (d), the dominant vibration frequencies are near to the natural frequencies of the plate where clearly visible chatter marks can be found on its surfaces; hence, chatters are induced. Traditional methods developed for single-mode vibration are difficult to achieve desired results as shown in this application. On the other hand, the proposed active control method designed to suppress multiple-mode vibrations overcomes common problems associated with traditional single-mode methods.

As proved in Section II, the unknown bound of disturbance is estimated by the adaptive law k, which dynamically adapts to the variation of the switching function. However, the estimated \hat{k} value [as depicted in Fig. 11(b)] increases gradually according to (14b) because chatter cannot be completely suppressed in practice, which is a common phenomenon in adaptive control [28]. To avoid excessively large value of \tilde{k} that could damage the PEA, an upper limit value was imposed on \hat{k} in all the active control experiments. In our paper, the upper limit kvalue is selected empirically by conducting experiments with the developed active control method. During experiments, the estimated value of \hat{k} is recorded without an upper limit value, while the PEA output is monitored simultaneously. If the PEA output is saturated, the experiment is stopped and the upper limit value can be selected, which is the current record value of \hat{k} . The effects of imposing an upper \hat{k} limit on the dynamic performance of the active control method can be illustrated numerically in Fig. 13 using numerical simulations of Cases A and B discussed in Section II-D. As shown in Fig. 13(a), the final values of the estimated k values (without setting the upper limit value) are 309 (Case A) and 323 (Case B). As shown in Fig. 13(b), the estimated \hat{k} values (with the upper limit value) after reaching the upper limit are kept at this limit along the entire evolution. Because of the upper limit that results in a "lower equivalent estimated \hat{k} value," the controlled system is "fooled"

by the lower than expected \hat{k} value. Thus, a reduced dynamic performance is expected when the imposed limit is reached. As numerically illustrated in Fig. 13(c), the displacements converge but slower to the steady states, demonstrating that the chatter can be suppressed under our developed method with a limit \hat{k} value. However, it exhibits a slow system convergence for chatter suppression as compared with Fig. 5 in Section II-D. The problem can be overcome by increasing the PEA output capacity. A potential alternative is to employ the projection algorithm with projection operator [29], [30] to redesign the adaptive laws to ensure the boundedness of the estimated value of \hat{k} .

As shown in Fig. 12(a) and (b), chatter cannot be suppressed by the PID control (with the same reconstructed displacement at the cutting point from the DFR as input); and clearly visible chatter marks can be found in the plate surfaces. These findings demonstrate the superiority of the proposed active control method over the conventional method.

IV. CONCLUSION

The design of an active control method, including an ASMC and the DFR, was proposed in this paper. Dedicated to chatter suppression of thin plates in turning, the dynamics of a rotating thin plate was modeled using a distributed-parameter approach. Different from existing active chatter controllers that rely on the lumped-parameter single-DOF cutting model, the effectiveness of the designed ASMC was theoretically analyzed and numerically illustrated with the distributed thin plate model. Parameter selection of the ASMC was discussed. The DFR was employed to capture the plate vibration during turning for displacement feedback of the ASMC. The active control method was evaluated via experiments on a lathe machine testbed. The results showed that the proposed method with the ASMC exhibits superior performance than the PID control and the conventional cutter without control. Particularly, the thin plate displacement was successfully reconstructed, and the plate chatter can be effectively attenuated under different working conditions with the proposed method. In contrast, the turning chatter could not be suppressed with the PID control and the conventional cutter without control.

APPENDIX

A. Elements of Dynamic Model

The elemental inertias **m**, damping **c**, and elasticity **k** in (3) are defined in (A1-3) where ρ , μ , E, and v are the density, damping coefficient, elastic modulus, and Poisson ratio of the material, and the moment of inertia is calculated by $I_2 = \rho h^3/12$

$$\mathbf{m} = \rho h - I_2 \nabla^2, \ \mathbf{c} = \mu, \ \mathbf{k} = \frac{Eh^3}{12(1 - v^2)} \nabla^2 \nabla^2.$$
 (A1-3)

In (A1), the Laplace operator ∇^2 is in polar coordinates

$$\nabla^2 = \frac{\partial^2}{\partial r^2} + \frac{\partial}{r\partial r} + \frac{\partial^2}{r^2 \partial \theta^2}.$$
 (A2)

For a constant spindle speed Ω , the centrifugal force f_l acting on the thin plate can be derived as follows:

$$f_{l} = -\frac{\rho h}{2} (r\Omega)^{2} \left(\nabla^{2} w + 2 \frac{\partial w}{r \partial r} \right) + q_{rr} \frac{\partial^{2} w}{\partial r^{2}}$$

$$+ q_{\theta\theta} \left(\frac{\partial w}{r \partial r} + \frac{\partial^{2} w}{r^{2} \partial \theta^{2}} \right) + q_{r\theta} \left(\frac{2\partial^{2} w}{r \partial r \partial \theta} - \frac{2\partial w}{r^{2} \partial \theta} \right)$$
(A3)

where $\mathbf{q} = [q_{rr} q_{\theta\theta} q_{r\theta}]^T$ is generated by the stress function [19].

B. Derivation of Dynamic Model in Modal Coordinates

Given the displacement field (4), the left side of (3) and the centrifugal force can be written in terms of $\phi_i(r, \theta)$ and $q_i(t)$ as

$$\sum_{i=0}^{k} \ddot{q}_{i} \left[\rho h - I_{2} \nabla^{2} \right] \phi_{i} + \mu \sum_{i=0}^{k} \dot{q}_{i} \phi_{i} + \bar{k}_{1} \sum_{i=0}^{k} q_{i} \nabla^{2} \nabla^{2} \phi_{i}$$
 (B1)

$$f_{l}(t; r, \theta; \Omega) = -\bar{k}_{2} \sum_{i=0}^{k} q_{i} \left(\nabla^{2} + \frac{2\partial}{r\partial r} \right) \phi_{i} + \sum_{i=0}^{k} q_{i} q_{rr} \frac{\partial^{2} \phi_{i}}{\partial r^{2}}$$

$$+ \sum_{i=0}^{k} q_{i} q_{\theta\theta} \left(\frac{\partial \phi_{i}}{r\partial r} + \frac{\partial^{2} \phi_{i}}{r^{2} \partial \theta^{2}} \right)$$

$$+ 2 \sum_{i=0}^{k} q_{i} q_{r\theta} \left(\frac{\partial^{2} \phi_{i}}{r\partial r \partial \theta} - \frac{\partial \phi_{i}}{r^{2} \partial \theta} \right)$$
(B2)

where

$$\bar{k}_1 = \frac{Eh^3}{12(1-v^2)} \text{ and } \bar{k}_2 = \frac{\rho h}{2}(r\Omega)^2.$$

Equation (3) becomes

$$\sum_{i=0}^{k} \ddot{q}_i(t) \left[\rho h - I_2 \nabla^2 \right] \phi_i(r,\theta) + \sum_{i=0}^{k} \mu \dot{q}_i(t) \phi_i(r,\theta)$$

$$+ \sum_{i=0}^{k} q_i(t) \Theta \phi_i(r,\theta) = \left[F_{ca}(t) + u(t) \right] \delta(r - r_p, \theta - \theta_p)$$
(P2)

where

$$\Theta = \bar{k}_1 \nabla^2 \nabla^2 + \bar{k}_2 \left(\nabla^2 + 2 \frac{\partial}{r \partial r} \right) - q_{rr} \frac{\partial^2}{\partial r^2} - q_{\theta\theta} \left(\frac{\partial}{r \partial r} + \frac{\partial^2}{r^2 \partial \theta^2} \right) - q_{r\theta} \left(\frac{2\partial^2}{r \partial r \partial \theta} - \frac{2\partial}{r^2 \partial \theta} \right).$$
(B3b)

Multiplying $\phi_i(r, \theta)$ in both sides of (B3a), integrating over r and θ , and using the orthogonality, (5a)–(5e) can be obtained.

REFERENCES

[1] M. Siddhpura and R. Paurobally, "A review of chatter vibration research in turning," *Int. J. Mach. Tools Manuf.*, vol. 61, pp. 27–47, Oct. 2012.

- [2] M. Stephens, A. Michael, C. Manzie, and C. Malcolm, "Model predictive control for reference tracking on an industrial machine tool servo drive," *IEEE Trans. Ind. Inf.*, vol. 9, no. 2, pp. 808–816, May 2013.
- [3] Y. Wu, H. Zhang, T. Huang, H. Zhao, and H. Ding, "Adaptive chatter mitigation control for machining processes with input saturations," *Int. J. Robust Nonlinear Control*, vol. 26, no. 14, pp. 3088–3100, Sep. 2015.
- [4] M. Chen and C. R. Knospe, "Control approaches to the suppression of machining chatter using active magnetic bearings," *IEEE Trans. Control* Syst. Technol., vol. 15, no. 2, pp. 220–232, Mar. 2007.
- [5] N. J. M. van Dijk, N. van de Wouw, and E. J. J. Doppenberg, "Robust active chatter control in the high-speed milling process," *IEEE Trans. Control Syst. Technol.*, vol. 20, no. 4, pp. 901–917, Jul. 2012.
- [6] F. Chen, M. Hanifzadegan, Y. Altintas, and X. Lu, "Active damping of boring bar vibration with a magnetic actuator," *IEEE/ASME Trans. Mecha*tron., vol. 20, no. 6, pp. 2783–2794, Feb. 2015.
- [7] A. Som, D. Kim, and H. Son, "Semiactive magnetorheological damper for high aspect ratio boring process," *IEEE/ASME Trans. Mechatron.*, vol. 20, no. 5, pp. 2575–2582, Feb. 2015.
- [8] X. Liu, C. Su, Z. Li, and Y. Fan, "FNN approximation-based active dynamic surface control for suppressing chatter in micro-milling with piezo-actuators," *IEEE Trans. Syst. Man Cybern.*, Syst., vol. 47, no. 8, pp. 2100–2113, Aug. 2017.
- [9] A. Ganguli, A. Deraemaeker, and A. Preumont, "Regenerative chatter reduction by active damping control," *J. Sound Vib.*, vol. 300, no. 3–5, pp. 847–862, Mar. 2007.
- [10] J. Munoa, I. Mancisidor, N. Loix, L. G. Uriarte, R. Barcena, and M. Zatarain, "Chatter suppression in ram type travelling column milling using a biaxial inertial actuator," *CIRP Ann. Manuf. Technol.*, vol. 62, no. 1, pp. 407–410, 2013.
- [11] J. L. Dohner et al., "Mitigation of chatter instabilities in milling by active structural control," J. Sound Vib., vol. 269, no. 1–2, pp. 197–211, Jan. 2004.
- [12] C. Mei, "Active regenerative chatter suppression during boring manufacturing process," *Robot. Comput. Integr. Manuf.*, vol. 21, no. 2, pp. 153–158, Apr. 2005
- [13] J. Monnin, F. Kuster, and K. Wegener, "Optimal control for chatter mitigation in milling-part 1: Modeling and control design," *Control Eng. Pract.*, vol. 24, pp. 156–166, Mar. 2014.
- [14] Z. Y. Chen, H. T. Zhang, X. M. Zhang, and H. Ding, "Adaptive active chatter control in milling processes," J. Dyn. Syst. Meas. Control Trans. ASME, vol. 136, no. 2, Dec. 2014, Art. no. 021007.
- [15] H. F. Ma, J. H. Wu, L. Yang, and Z. H. Xiong, "Active chatter suppression with displacement-only measurement in turning process," *J. Sound Vib.*, vol. 401, pp. 255–267, Aug. 2017.
- [16] Y. Zhang and N. D. Sims, "Milling workpiece chatter avoidance using piezoelectric active damping: A feasibility study," *Smart Mater. Struct.*, vol. 14, no. 6, pp. N65–N70, Dec. 2005.
- [17] H. Moradi, F. Bakhtiari-Nejad, and M. R. Movahhedy, "Tuneable vibration absorber design to suppress vibrations: An application in boring manufacturing process," *J. Sound Vib.*, vol. 318, no. 1–2, pp. 93–108, Nov. 2008.
- [18] J. Munoa et al., "Chatter suppression techniques in metal cutting," CIRP Ann. Manuf. Techn., vol. 65, no. 2, pp. 785–808, 2016.
- [19] J. Guo, W. Liu, and K.-M. Lee, "Displacement field sensing and reconstruction for vibration of a thin-wall plate," in *Proc. IEEE/ASME Int. Conf. Adv. Intell. Mechatron.* (AIM), 2015, pp. 1350–1355.
- [20] A. Bartoszewicz, "A new reaching law for sliding mode control of continuous time systems with constraints," *Trans. Inst. Meas. Control*, vol. 37, no. 4, pp. 515–521, Apr. 2015.
- [21] G. Stepan, A. Kiss, B. Ghalamchi, J. Sopanen, and D. Bachrathy, "Chatter avoidance in cutting highly flexible workpiece," *CIRP Ann. Manuf. Technol.*, vol. 66, no. 1, pp. 377–380, 2017.
- [22] C. Chen and Y. Tsao, "A stability analysis of turning a tailstock supported flexible workpiece," *Int. J. Mach. Tools Manuf.*, vol. 46, no. 1, pp. 18–25, Jan. 2006
- [23] Y. Man, J. Guo, and K.-M. Lee, "A modal expansion method for displacement and strain field reconstruction of a thin-wall component during machining," *IEEE/ASME Trans. Mechatron.*, vol. 23, no. 3, pp. 1028–1037, Jun. 2018.
- [24] Q. Hu, "Robust adaptive sliding mode attitude maneuvering and vibration damping of three-axis-stabilized flexible spacecraft with actuator saturation limits," *Nonlinear Dyn.*, vol. 55, no. 4, pp. 301–321, Mar. 2009.
- [25] P. Li, X. Yu, and B. Xiao, "Adaptive quasi-optimal higher order sliding mode control without gain overestimation," *IEEE Trans. Ind. Inf.*, vol. 9, no. 2, pp. 1–9, Dec. 2017.

- [26] Z. Zhu, Y. Xia, and M. Fu, "Adaptive sliding mode control for attitude stabilization with actuator saturation," *IEEE Trans. Ind. Electron.*, vol. 58, no. 10, pp. 4898–4907, Oct. 2011.
- [27] G. Gu and L. Zhu, "Motion control of piezoceramic actuators with creep, hysteresis and vibration compensation," *Sens. Actuators A Phys.*, vol. 197, no. 1, pp. 76–87, Aug. 2013.
- [28] K. J. Astrom and B. Wittenmark, Adaptive Control. Reading, MA: Addison-Wesley, 1989.
- [29] J. Pomet and L. Praly, "Adaptive nonlinear regulation: Estimation from the Lyapunov equation," *IEEE Trans. Autom. Control*, vol. 37, no. 6, pp. 729–740, Jun. 1992.
- [30] G. Goodwin and K. Sin, *Adaptive Filtering, Prediction and Control.* Englewood Cliffs, NJ: Prentice-Hall, 1984.



Jianhua Wu (M'13) received the B.E. degree in engineering mechanics and the Ph.D. degree in mechatronics from Shanghai Jiao Tong University, Shanghai, China, in 2002 and 2007, respectively.

He is currently an Associate Professor with the State Key Laboratory of Mechanical System and Vibration, School of Mechanical Engineering, Shanghai Jiao Tong University, Shanghai, China. His research interests include high-speed and high-precision motion control,

high-performance motor driver design, and servo self-tuning technology, which are applied to numerical control systems.



Haifeng Ma received the B.E. and M.E. degrees in mechanical engineering from Southwest Jiaotong University, Chengdu, China, in 2010 and 2013, respectively, and the Ph.D. degree in mechatronics from Shanghai Jiao Tong University, Shanghai, China, in 2017.

He is currently working with the Key Laboratory of High Efficiency and Clean Mechanical Manufacture, Ministry of Education, School of Mechanical Engineering, Shandong University, Jinan, China. He is also a Hong Kong Scholar

Postdoctoral Fellow in The Hong Kong Polytechnic University, Kowloon, Hong Kong, China. His research interests include sliding-mode control and intelligent manufacturing.



Zhenhua Xiong (M'11) received the B.E. and M.E. degrees in aircraft design and vibration engineering from the Department of Aircraft Design, Nanjing University of Aeronautics and Astronautics, Nanjing, China, in 1995 and 1998, respectively, and the Ph.D. degree in mechatronics from the Department of Electrical and Electronics Engineering, Hong Kong University of Science and Technology, Clear Water Bay, Hong Kong, in 2002.

He is currently a Professor with the State Key Laboratory of Mechanical System and Vibration, School of Mechanical Engineering, Shanghai Jiao Tong University, Shanghai, China. His research interests include servo motion control and intelligent manufacturing.



Jiajie Guo (M'12) received the B.S. degree in theoretical and applied mechanics from the Department of Engineering Mechanics and Science, Peking University, Beijing, China, in 2006, and M.S. and Ph.D. degrees in mechanical engineering from the Department of Mechanical Engineering, Georgia Institute of Technology, Atlanta, GA, USA, in 2009 and 2011, respectively.

He is currently an Associate Professor with the State Key Laboratory of Digital Manufacturing Equipment and Technology, the School of

Mechanical Science and Engineering, Huazhong University of Science and Technology, Wuhan, China. His current research interests include mechatronics, robotics, and system dynamics/control.



Kok-Meng Lee (M'89–SM'02–F'05) received the B.S. degree in mechanical engineering from the State University of New York, Buffalo, NY, USA, in 1980, and the M.S. and Ph.D. degrees in mechanical engineering from the Massachusetts Institute of Technology, Cambridge, MA, USA, in 1982 and 1985, respectively.

He is currently a Professor with the George W. Woodruff School of Mechanical Engineering, Georgia Institute of Technology, Atlanta, GA, USA. He is also a Distinguished Professor with

the State Key Laboratory of Digital Manufacturing Equipment and Technology, Huazhong University of Science and Technology, Wuhan, China. He holds eight patents in machine vision, three degrees-of-freedom spherical motor/encoder, and live-bird handling system. His research interests include system dynamics/control, robotics, automation, and mechatronics.

Dr. Lee is a Fellow of the American Society of Mechanical Engineers (ASME). He is the Founding Editor-in-Chief of *Springer International Journal of Intelligent Robotics and Applications*. He received the National Science Foundation Presidential Young Investigator, the Sigma Xi Junior Faculty Research, the International Hall of Fame New Technology, the Kayamori Best Paper Awards, the TMech Best Paper Award, and the Michael J. Rabin Leadership Award. He was also honored as a Pao Yu-Kong Chair Professor at Zhejiang University, Hangzhou, China.